Quantum Phase Transitions at Integer Filling

Subir Sachdev

Department of Physics, Harvard University,
Cambridge, Massachusetts, 02138, USA and
Perimeter Institute for Theoretical Physics,
Waterloo, Ontario N2L 2Y5, Canada

(Dated: March 1, 2016)

Abstract

Notes adapted from

Quantum Phase Transitions by S. Sachdev, Cambridge University Press, and

String Theory and Its Applications, TASI 2010, From meV to the Planck Scale, Proceedings of the 2010 Theoretical Advanced Study Institute in Elementary Particle Physics, Boulder, Colorado, 1-25 June 2010, World Scientific (2011), arXiv:1012.0299.

CONTENTS

I. BOSON HUBBARD MODEL

The boson Hubbard model describes bosons moving on a lattice with on-site repulson.

We introduce the boson operator $\hat{b}_i$, which annihilates bosons on the sites, i, of a regular lattice in d dimensions. These Bose operators and their Hermitian conjugate creation operators obey the commutation relation

$$\left[\hat{b}_i, \hat{b}_j^\dagger\right] = \delta_{ij}, \tag{1}$$

while two creation or annihilation operators always commute. It is also useful to introduce the boson number operator

$$\hat{n}_{bi} = \hat{b}_i^\dagger \hat{b}_i, \tag{2}$$

which counts the number of bosons on each site. We allow an arbitrary number of bosons on each site. Thus the Hilbert space consists of states $|\{m_j\}\rangle$, that are eigenstates of the number operators

$$\hat{n}_{bi}|\{m_j\}\rangle = m_i|\{m_j\}\rangle, \tag{3}$$

and every m_j in the set $\{m_j\}$ is allowed to run over all nonnegative integers. This includes the "vacuum" state with no bosons at all $|\{m_j = 0\}\rangle$.

The Hamiltonian of the boson Hubbard model is

$$H_B = -w \sum_{\langle ij \rangle} \left(\hat{b}_i^\dagger \hat{b}_j + \hat{b}_j^\dagger \hat{b}_i \right) - \mu \sum_i \hat{n}_{bi} + (U/2) \sum_i \hat{n}_{bi}(\hat{n}_{bi} - 1). \tag{4}$$

The first term, proportional to w, allows hopping of bosons from site to site ($\langle ij \rangle$ represents nearest neighbor pairs); if each site represents a superconducting grain, then w is the Josephson tunneling that allows Cooper pairs to move between grains. The second term, μ, represents the chemical potential of the bosons: Changing in the value of μ changes the total number of bosons. Depending upon the physical conditions, a given system can either be constrained to be at a fixed chemical potential (the grand canonical ensemble) or have a fixed total number of bosons (the canonical ensemble). Theoretically it is much simpler to consider the fixed chemical potential case, and results at fixed density can always be obtained from them after a Legendre transformation. Finally, the last term, $U > 0$, represents the simplest possible repulsive interaction between the bosons. We have taken only an on-site repulsion. This can be considered to be the charging energy of each superconducting grain. Off-site and longer-range repulsion are undoubtedly important in realistic systems, but these are neglected in this simplest model.

The Hubbard model H_B is invariant under a global U(1) $\equiv$ O(2) phase transformation under which

$$\hat{b}_i \to \hat{b}_i e^{i\phi}. \tag{5}$$

This symmetry is related to the conservation of the total number of bosons

$$\hat{N}_b = \sum_i \hat{n}_{bi}; \tag{6}$$

it is easily verified that $\hat{N}_b$ commutes with $\hat{H}$.

We will begin our study of H_B by introducing a simple mean-field theory in Section I A. The coherent state path integral representation of the boson Hamiltonian will then be developed in Section I B. The continuum quantum theories describing fluctuations near the quantum critical points will be introduced in Section I C. Our treatment builds on the work of Fisher *et al.* [1].

A. Mean field theory

The strategy, as in any mean-field theory, will be to model the properties of H_B by the best possible sum, $H_{\rm MF}$, of single-site Hamiltonians:

$$H_{\rm MF} = \sum_i \left(-\mu \hat{n}_{bi} + (U/2)\, \hat{n}_{bi}(\hat{n}_{bi} - 1) - \Psi_B^* \hat{b}_i - \Psi_B \hat{b}_i^\dagger \right), \tag{7}$$

where the complex number Ψ_B is a variational parameter. We have chosen a mean-field Hamiltonian with the same on-site terms as H_B and have added an additional term with a "field" Ψ_B to

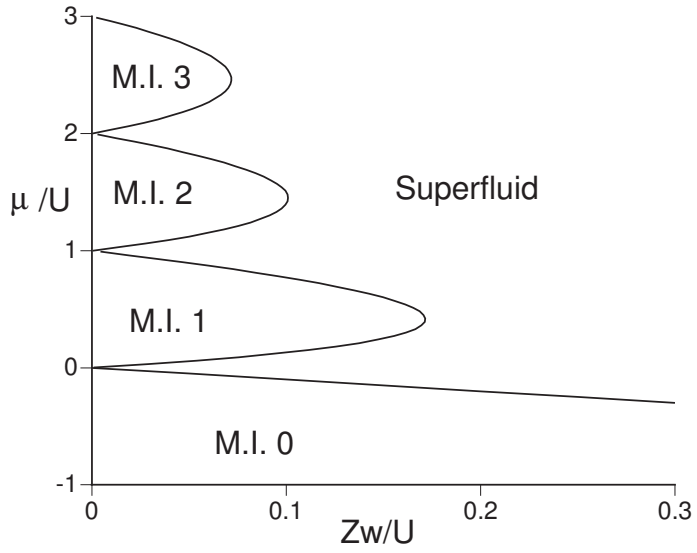

FIG. 1. Mean-field phase diagram of the ground state of the boson Hubbard model H_B in (4). The notation M.I. n refers to a Mott insulator with $n_0(\mu/U) = n$.

represent the influence of the neighboring sites; this field has to be self-consistently determined. Notice that this term breaks the U(1) symmetry and does not conserve the total number of particles. This is to allow for the possibility of broken-symmetric phases, whereas symmetric phases will appear at the special value $\Psi_B = 0$. As we saw in the analysis of H_R, the state that breaks the U(1) symmetry will have a nonzero stiffness to rotations of the order parameter; in the present case this stiffness is the superfluid density characterizing a superfluid ground state of the bosons.

Another important assumption underlying (7) is that the ground state does not spontaneously break a translational symmetry of the lattice, as the mean-field Hamiltonian is the same on every site. Such a symmetry breaking is certainly a reasonable possibility, but we will ignore this complication here for simplicity.

We will determine the optimum value of the mean-field parameter Ψ_B by a standard procedure. First, determine the ground state wavefunction of $H_{\rm MF}$ for an arbitrary Ψ_B; because $H_{\rm MF}$ is a sum of single-site Hamiltonians, this wavefunction will simply be a product of single-site wavefunctions. Next, evaluate the expectation value of H_B in this wavefunction. By adding and subtracting $H_{\rm MF}$ from H_B, we can write the mean-field value of the ground state energy of H_B in the form

$$\frac{E_0}{M} = \frac{E_{\rm MF}(\Psi_B)}{M} - Zw\langle\hat{b}^\dagger\rangle\langle\hat{b}\rangle + \langle\hat{b}\rangle\Psi_B^* + \langle\hat{b}^\dagger\rangle\Psi_B, \tag{8}$$

where $E_{\rm MF}(\Psi_B)$ is the ground state energy of $H_{\rm MF}$, M is the number of sites of the lattice, Z is the number of nearest neighbors around each lattice point (the "coordination number"), and the expectation values are evaluated in the ground state of $H_{\rm MF}$. The final step is to minimize (8) over variations in Ψ_B. We have carried out this step numerically and the results are shown in Fig. 1.

Notice that even on a single site, $H_{\rm MF}$ has an infinite number of states, corresponding to the allowed values $m \geq 0$ of the integer number of bosons on each site. The numerical procedure necessarily truncates these states at some large occupation number, but the errors are not difficult to control. In any case, we will show that all the essential properties of the phase diagram can be obtained analytically. Also, by taking the derivative of (8) with respect to Ψ_B, it is easy to show that at the optimum value of Ψ_B

$$\Psi_B = Zw\langle\hat{b}\rangle; \tag{9}$$

this relation, however, does not hold at a general point in parameter space.

First, let us consider the limit $w=0$. In this case the sites are decoupled, and the mean-field theory is exact. It is also evident that $\Psi_B = 0$, and we simply have to minimize the on-site interaction energy. The on-site Hamiltonian contains only the operator $\hat{n}$, and the solution involves finding the boson occupation number (which are the integer-valued eigenvalues of $\hat{n}$) that minimizes H_B. This is simple to carry out, and we get the ground state wavefunction

$$|m_i = n_0(\mu/U)\rangle\,, \tag{10}$$

where the integer-valued function $n_0(\mu/U)$ is given by

$$n_0(\mu/U) = \begin{cases} 0, & \text{for } \mu/U < 0, \\ 1, & \text{for } \quad 0 < \mu/U < 1, \\ 2, & \text{for } 1 < \mu/U < 2, \\ \vdots & \vdots \\ n, & \text{for } n-1 < \mu/U < n. \end{cases} \tag{11}$$

Thus each site has exactly the same integer number of bosons, which jumps discontinuously whenever μ/U goes through a positive integer. When μ/U is exactly equal to a positive integer, there are two degenerate states on each site (with boson numbers differing by 1) and so the entire system has a degeneracy of 2^M. This large degeneracy implies a macroscopic entropy; it will be lifted once we turn on a nonzero w.

We now consider the effects of a small nonzero w. As is shown in Fig. 1, the regions with $\Psi_B = 0$ survive in lobes around each $w = 0$ state (10) characterized by a given integer value of $n_0(\mu/U)$. Only at the degenerate point with $\mu/U =$ integer does a nonzero w immediately lead to a state with $\Psi_B \neq 0$. We will consider the properties of this $\Psi_B \neq 0$ later, but now we discuss the properties of the lobes with $\Psi_B = 0$ in some more detail. In mean-field theory, these states have wavefunctions still given exactly by (10). However, it is possible to go beyond mean-field theory and make an important exact statement about each of the lobes: The expectation value of the number of bosons in each site is given by

$$\left\langle \hat{b}_i^\dagger \hat{b}_i \right\rangle = n_0(\mu/U), \tag{12}$$

which is the same result one would obtain from the product state (10) (which, we emphasize, is not the exact wavefunction for $w \neq 0$). There are two important ingredients behind the result (12): the existence of an energy gap and the fact that $\hat{N}_b$ commutes with H_B. First, recall that at $w = 0$, provided μ/U was not exactly equal to a positive integer, there was a unique ground state, and there was a nonzero energy separating this state from all other states (this is the energy gap). As a result, when we turn on a small nonzero w, the ground state will move adiabatically without undergoing any level crossings with any other state. Now the $w = 0$ state is an exact eigenstate of $\hat{N}_b$ with eigenvalue $Mn_0(\mu/U)$, and the perturbation arising from a nonzero w commutes with $\hat{N}_b$. Consequently, the ground state will remain an eigenstate of $\hat{N}_b$ with precisely the same eigenvalue, $Mn_0(\mu/U)$, even for small nonzero w. Assuming translational invariance, we then immediately have the exact result (12). Notice that this argument also shows that the energy gap above the ground state will survive everywhere within the lobe. These regions with a quantized value of the density and an energy gap to all excitations are known as "Mott insulators." Their ground states are very similar to, but not exactly equal to, the simple state (10): They involve in addition terms with bosons undergoing virtual fluctuations between pairs of sites, creating particle–hole pairs. The Mott insulators are also known as "incompressible" because their density does not change under changes of the chemical potential μ or other parameters in H_B:

$$\frac{\partial \langle \hat{N}_b \rangle}{\partial \mu} = 0. \tag{13}$$

It is worth reemphasizing here the remarkable nature of the exact result (12). From the perspective of classical critical phenomena, it is most unusual to find the expectation value of any observable to be pinned at a quantized value over a finite region of the phase diagram. However, as we will see, quantum field theories of a certain structure allow such a phenomenon, and we will meet different realizations of it in subsequent chapters. The existence of observables such as $\hat{N}_b$ that commute with the Hamiltonian is clearly a crucial ingredient.

The numerical analysis shows that the boundary of the Mott insulating phases is a second-order quantum phase transition (i.e., a nonzero Ψ_B turns on continuously). With the benefit of this knowledge, we can determine the positions of the phase boundaries. By the usual Landau theory argument, we simply need to expand E_0 in (8) in powers of Ψ_B,

$$E_0 = E_{00} + r|\Psi_B|^2 + \mathcal{O}(|\Psi_B|^4), \tag{14}$$

and the phase boundary appears when r changes sign. The value of r can be computed from (8) and (7) by second-order perturbation theory, and we find

$$r = \chi_0(\mu/U)\left[1 - Zw\chi_0(\mu/U)\right], \tag{15}$$

where

$$\chi_0(\mu/U) = \frac{n_0(\mu/U) + 1}{Un_0(\mu/U) - \mu} + \frac{n_0(\mu/U)}{\mu - U(n_0(\mu/U) - 1)}. \tag{16}$$

The function $n_0(\mu/U)$ in (11) is such that the denominators in (16) are positive, except at the points at which boson occupation number jumps at $w = 0$. The solution of the simple equation $r = 0$ leads to the phase boundaries shown in Fig. 1.

Finally, we turn to the phase with $\Psi_B \neq 0$. The mean-field parameter Ψ_B varies continuously as the parameters are varied. As a result all thermodynamic variables also change, and the density does not take a quantized value; by a suitable choice of parameters, the average density can be varied smoothly across any real positive value. So this is a compressible state in which

$$\frac{\partial \langle \hat{N}_b \rangle}{\partial \mu} \neq 0. \tag{17}$$

As we noted earlier, the presence of a $\Psi_B \neq 0$ implies that the U(1) symmetry is broken, and there is a nonzero stiffness (*i.e.* helicity modulus) to twists in the orientation of the order parameter.

We also note that extensions of the boson Hubbard model with interactions beyond nearest neighbor can spontaneously break translational symmetry at certain densities. If this symmetry breaking coexists with the superfluid order, one can obtain a "supersolid" phase.

B. Coherent state path integral

To avoid inessential indices, we present the derivation of the coherent state path integral by focusing on a single site, and drop the site index. We will first derive the result in a general notation, to allow subsequent application to quantum spin systems. So we consider a general Hamiltonian $H(\hat{\mathbf{S}})$, dependent upon operators $\hat{\mathbf{S}}$ which need not commute with each other. So for the boson Hubbard model, $\hat{\mathbf{S}}$ is a two-dimensional vector of operators $\hat{b}$ and $\hat{b}^\dagger$ which obey (1). When we apply the results to quantum spin systems, $\hat{\mathbf{S}}$ represents the usual spin operators $\hat{S}_{x,y,z}$.

Our first step is to introduce the coherent states. These are an infinite set of states $|\mathbf{N}\rangle$, labeled by the a continuous vector $\mathbf{N}$ (in 2 or 3 dimensions for the two cases above). They are normalized to unity,

$$\langle \mathbf{N}|\mathbf{N}\rangle = 1, \tag{18}$$

but are not orthogonal $\langle \mathbf{N}|\mathbf{N}'\rangle \neq 0$ for $\mathbf{N} \neq \mathbf{N}'$. They do, however, satisfy a completeness relation

$$\mathcal{C}_N \int d\mathbf{N}\, |\mathbf{N}\rangle\langle \mathbf{N}| = 1 \tag{19}$$

where $\mathcal{C}_N$ is a normalization constant. Because of their nonorthogonality, these states are called "over-complete." Finally, they are chosen with a useful property: the diagonal expectation values of the operators $\hat{\mathbf{S}}$ are very simple:

$$\langle \mathbf{N}|\hat{\mathbf{S}}|\mathbf{N}\rangle = \mathbf{N}. \tag{20}$$

This property implies that the vector $\mathbf{N}$ is a classical approximation to the operators $\hat{\mathbf{S}}$. The relations (18), (19), and (20) define the coherent states, and are all we will need here to set up the coherent state path integral.

We also need the diagonal matrix elements of the Hamiltonian in the coherent state basis. Usually, it is possible to arrange the operators such that

$$\langle \mathbf{N}|H(\hat{\mathbf{S}})|\mathbf{N}\rangle = H(\mathbf{N}); \tag{21}$$

i.e. $H(\mathbf{N})$ has the same functional dependence upon $\mathbf{N}$ as the original Hamiltonian has on $\mathbf{S}$. For the boson Hubbard model, this corresponds, as we will see, to normal-ordering the creation and annihilation operators. In any case, the right-hand-side could have a distinct functional dependence on $\mathbf{N}$, but we will just refer to the diagonal matrix element as above.

We proceed to the derivation of the coherent state path integral for the partition function

$$\mathcal{Z} = \mathrm{Tr}\exp(-H(\hat{\mathbf{S}})/T). \tag{22}$$

We break up the exponential into a large number of exponentials of infinitesimal time evolution operators

$$\mathcal{Z} = \lim_{M\to\infty}\prod_{i=1}^{M}\exp(-\Delta\tau_i H(\hat{\mathbf{S}})), \tag{23}$$

where $\Delta\tau_i = 1/MT$, and insert a set of coherent states between each exponential by using the identity (19); we label the state inserted at a "time" τ by $|\mathbf{N}(\tau)\rangle$. We can then evaluate the expectation value of each exponential by use of the identity (20)

$$\begin{aligned}
&\langle \mathbf{N}(\tau)|\exp(-\Delta\tau H(\hat{\mathbf{S}}))|\mathbf{N}(\tau-\Delta\tau)\rangle \\
&\quad\approx \langle \mathbf{N}(\tau)|(1-\Delta\tau H(\hat{\mathbf{S}}))|\mathbf{N}(\tau-\Delta\tau)\rangle \\
&\quad\approx 1-\Delta\tau\langle \mathbf{N}(\tau)|\frac{d}{d\tau}|\mathbf{N}(\tau)\rangle - \Delta\tau H(\mathbf{N}) \\
&\quad\approx \exp\left(-\Delta\tau\langle \mathbf{N}(\tau)|\frac{d}{d\tau}|\mathbf{N}(\tau)\rangle - \Delta\tau H(\mathbf{N})\right).
\end{aligned} \tag{24}$$

In each step we have retained expressions correct to order $\Delta\tau$. Because the coherent states at time τ and $\tau+\Delta\tau$ can in principle have completely different orientations, a priori, it is not clear that expanding these states in derivatives of time is a valid procedure. This is a subtlety that afflicts all coherent state path integrals and has been discussed more carefully by Negele and Orland [2]. The conclusion of their analysis is that except for the single "tadpole" diagram where a point-splitting of time becomes necessary, this expansion in derivatives of time always leads to correct results. In any case, the resulting coherent state path integral is a formal expression that cannot be directly evaluated, and in case of any doubt one should always return to the original discrete time product in (23).

Keeping in mind the above caution, we insert (24) into (23), take the limit of small $\Delta\tau$, and obtain the following functional integral for $\mathcal{Z}$:

$$\mathcal{Z} = \int_{\mathbf{N}(0)=\mathbf{N}(1/T)}\mathcal{D}\mathbf{N}(\tau)\exp\left\{-\mathcal{S}_B - \int_0^{1/T} d\tau H(\mathbf{N}(\tau))\right\}, \tag{25}$$

where

$$\mathcal{S}_B = \int_0^{1/T} d\tau \langle \mathbf{N}(\tau)| \frac{d}{d\tau} |\mathbf{N}(\tau)\rangle \tag{26}$$

and $H(S\mathbf{N})$ is obtained by replacing every occurrence of $\hat{\mathbf{S}}$ in the Hamiltonian by $S\mathbf{N}$. The promised Berry phase term is S_B, and it represents the overlap between the coherent states at two infinitesimally separated times. It can be shown straightforwardly from the normalization condition, $\langle \mathbf{N}|\mathbf{N}\rangle = 1$, that $\mathcal{S}_B$ is pure imaginary.

1. *Boson coherent states*

We now apply the general formalism above to the boson Hubbard model. As before, we drop the site index i.

For the state label, we replace the two-dimensional vector $\mathbf{N}$ by a complex number ψ, and so the coherent states are $|\psi\rangle$, with one state for every complex number. A state with the properties (18), (19), and (20) turns out to be

$$|\psi\rangle = e^{-|\psi|^2/2} \exp\left(\psi \hat{b}^\dagger\right) |0\rangle \tag{27}$$

where $|0\rangle$ is the boson vacuum state (one of the states in (3)). This state is normalized as required by (18), and we can now obtain its diagonal matrix element

$$\begin{aligned} \langle \psi | \hat{b} | \psi \rangle &= e^{-|\psi|^2} \frac{\partial}{\partial \psi^*} \langle 0| \, e^{\psi^* \hat{b}} \, e^{\psi \hat{b}^\dagger} \, |0\rangle \\ &= e^{-|\psi|^2} \frac{\partial}{\partial \psi^*} e^{|\psi|^2} = \psi, \end{aligned} \tag{28}$$

which satisfies the requirement (20). For the complete relation, we evaluate

$$\begin{aligned} \int d\psi d\psi^* |\psi\rangle\langle\psi| &= \sum_{n=0}^{\infty} \frac{|n\rangle\langle n|}{n!} \int d\psi d\psi^* |\psi|^{2n} e^{-|\psi|^2} \\ &= \pi \sum_{n=0}^{\infty} |n\rangle\langle n| \end{aligned} \tag{29}$$

where $|n\rangle$ are the number states in (3), $d\psi d\psi^* \equiv d\mathrm{Re}(\psi) d\mathrm{Im}(\psi)$, and we have picked only the diagonal terms in the double sum over number states because the off-diagonal terms vanish after the angular ψ integration. This result identifies $\mathcal{C}_N = 1/\pi$. So we have satisfied the properties (18), (19), and (20) required of all coherent states.

For the path integral, we need the Berry phase term in (26). This is a path integral over trajectories in the complex plane, $\psi(\tau)$, and we have

$$\langle \psi(\tau)| \frac{d}{d\tau} |\psi(\tau)\rangle = e^{-|\psi(\tau)|^2} \langle 0| e^{\psi^*(\tau)\hat{b}} | \frac{d}{d\tau} | e^{\psi(\tau)\hat{b}^\dagger} |0\rangle = \psi^* \frac{d\psi}{d\tau}. \tag{30}$$

We are now ready to combine (30) and (25) to obtain the coherent state path integral of the boson Hubbard model.

C. Continuum quantum field theories

Returning to our discussion of the boson Hubbard model, here we will describe the low-energy properties of the quantum phase transitions between the Mott insulators and the superfluid found in Section I A. We will find that it is crucial to distinguish between two different cases, each characterized by its own universality class and continuum quantum field theory. The important diagnostic distinguishing the two possibilities will be the behavior of the boson density across the transition. In the Mott insulator, this density is of course always pinned at some integer value. As one undergoes the transition to the superfluid, depending upon the precise location of the system in the phase diagram of Fig. 1, there are two possible behaviors of the density: (A) The density remains pinned at its quantized value in the superfluid in the vicinity of the quantum critical point, or (B) the transition is accompanied by a change in the density.

We begin by writing the partition function of H_B, $\mathcal{Z}_B = \mathrm{Tr} e^{-H_B/T}$ in the coherent state path integral representation derived in Section I B:

$$\begin{aligned} \mathcal{Z}_B &= \int \mathcal{D}b_i(\tau)\mathcal{D}b_i^\dagger(\tau) \exp\left(-\int_0^{1/T} d\tau \mathcal{L}_b\right), \\ \mathcal{L}_b &= \sum_i \left(b_i^\dagger \frac{db_i}{d\tau} - \mu b_i^\dagger b_i + (U/2)\, b_i^\dagger b_i^\dagger b_i b_i\right) - w\sum_{\langle ij\rangle}\left(b_i^\dagger b_j + b_j^\dagger b_i\right). \end{aligned} \tag{31}$$

Here we have changed notation $\psi(\tau) \to b(\tau)$, as is conventional; we are dealing exclusively with path integrals from now on, and so there is no possibility of confusion with the operators $\hat{b}$ in the Hamiltonian language. Also note that the repulsion proportional to U in (4) becomes the product of four boson operators above after normal ordering, and we can then use (21).

It is clear that the critical field theory of the superfluid-insulator transition should be expressed in terms of a spacetime-dependent field $\Psi_B(x,\tau)$, which is analogous to the mean-field parameter Ψ_B appearing in Section I A. Such a field is most conveniently introduced by the well-known Hubbard–Stratanovich transformation on the coherent state path integral. We decouple the hopping term proportional to w by introducing an auxiliary field $\Psi_{Bi}(\tau)$ and transforming $\mathcal{Z}_B$ to

$$\begin{aligned} \mathcal{Z}_B &= \int \mathcal{D}b_i(\tau)\mathcal{D}b_i^\dagger(\tau)\mathcal{D}\Psi_{Bi}(\tau)\mathcal{D}\Psi_{Bi}^\dagger(\tau) \exp\left(-\int_0^{1/T} d\tau \mathcal{L}_b'\right), \\ \mathcal{L}_b' &= \sum_i \left(b_i^\dagger \frac{db_i}{d\tau} - \mu b_i^\dagger b_i + (U/2)\, b_i^\dagger b_i^\dagger b_i b_i - \Psi_{Bi} b_i^\dagger - \Psi_{Bi}^* b_i\right) \\ &\quad + \sum_{i,j} \Psi_{Bi}^* w_{ij}^{-1} \Psi_{Bj}. \end{aligned} \tag{32}$$

We have introduced the symmetric matrix w_{ij} whose elements equal w if i and j are nearest neighbors and vanish otherwise. The equivalence between (32) and (31) (sometimes called the

Hubbard–Stratanovich transformation) can be easily established by simply carrying out the Gaussian integral over Ψ_B; this also generates some overall normalization factors, but these have been absorbed into a definition of the measure $\mathcal{D}\Psi_B$. Let us also note a subtlety we have glossed over: Strictly speaking, the transformation between (32) and (31) requires that all the eigenvalues of w_{ij} be positive, for only then are the Gaussian integrals over Ψ_B well defined. This is not the case for, say, the hypercubic lattice, which has negative eigenvalues for w_{ij}. This can be repaired by adding a positive constant to all the diagonal elements of w_{ij} and subtracting the same constant from the on-site b part of the Hamiltonian. We will not explicitly do this here as our interest is only in the long-wavelength modes of the Ψ_B field, and the corresponding eigenvalues of w_{ij} are positive.

For our future purposes, it is useful to describe an important symmetry property of (32). Notice that the functional integrand is invariant under the following time-dependent U(1) gauge transformation:

$$\begin{aligned} b_i &\to b_i e^{i\phi(\tau)}, \\ \Psi_{Bi} &\to \Psi_{Bi} e^{i\phi(\tau)}, \\ \mu &\to \mu + i\frac{\partial \phi}{\partial \tau}. \end{aligned} \tag{33}$$

The chemical potential μ becomes time dependent above, and so this transformation takes one out of the physical parameter regime; nevertheless (33) is very useful, as it places important restrictions on subsequent manipulations of $\mathcal{Z}_B$.

The next step is to integrate out the b_i, $b_i^\dagger$ fields from (32). This can be done exactly in powers of Ψ_B and Ψ_B^*: The coefficients are simply products of Green's functions of the b_i. The latter can be determined in closed form because the Ψ_B-independent part of $\mathcal{L}_b'$ is simply a sum of single-site Hamiltonians for the b_i: these were exactly diagonalized in (10), and all single-site Green's functions can also be easily determined. We re-exponentiate the resulting series in powers of Ψ_B, Ψ_B^* and expand the terms in spatial and temporal gradients of Ψ_B. The expression for $\mathcal{Z}_B$ can now be written as [1]

$$\mathcal{Z}_B = \int \mathcal{D}\Psi_B(x,\tau)\mathcal{D}\Psi_B^*(x,\tau) \exp\left(-\frac{V\mathcal{F}_0}{T} - \int_0^{1/T} d\tau \int d^d x \mathcal{L}_B \right), \tag{34}$$

$$\mathcal{L}_B = K_1 \Psi_B^* \frac{\partial \Psi_B}{\partial \tau} + K_2 \left| \frac{\partial \Psi_B}{\partial \tau} \right|^2 + K_3 \left| \nabla \Psi_B \right|^2 + \tilde{r} |\Psi_B|^2 + \frac{u}{2} |\Psi_B|^4 + \cdots .$$

Here $V = Ma^d$ is the total volume of the lattice, and a^d is the volume per site. The quantity $\mathcal{F}_0$ is the free energy density of a system of decoupled sites; its derivative with respect to the chemical potential gives the density of the Mott insulating state, and so

$$-\frac{\partial \mathcal{F}_0}{\partial \mu} = \frac{n_0(\mu/U)}{a^d}. \tag{35}$$

The other parameters in (34) can also be expressed in terms of μ, U, and w but we will not display explicit expressions for all of them. Most important is the parameter $\tilde{r}$, which can be seen to be

$$\tilde{r}a^d = \frac{1}{Zw} - \chi_0(\mu/U), \tag{36}$$

where χ_0 was defined in (16). Notice that $\tilde{r}$ is proportional to the mean-field r in (15); in particular, $\tilde{r}$ vanishes when r vanishes, and the two quantities have the same sign. The mean-field critical point between the Mott insulator and the superfluid appeared at $r = 0$, and it is not surprising that the mean-field critical point of the continuum theory (34) is given by the same condition.

Of the other couplings in (34), K_1, the coefficient of the first-order time derivative also plays a crucial role. It can be computed explicitly, but it is simpler to note that the value of K_1 can be fixed by demanding that (34) be invariant under (33) for small ϕ: A simple calculation shows that we must have

$$K_1 = -\frac{\partial \tilde{r}}{\partial \mu}. \tag{37}$$

This relationship has a very interesting consequence. Notice that K_1 vanishes when $\tilde{r}$ is μ-independent; however, this is precisely the condition that the Mott insulator–superfluid phase boundary in Fig. 1 have a vertical tangent (i.e., at the tips of the Mott insulating lobes). This is significant because at the value $K_1 = 0$ (34) is a *relativistic* field theory for a complex scalar field Ψ_B So the Mott insulator to superfluid transition is in the universality class of a relativistic scalar field theory for $K_1 = 0$. In contrast, for $K_1 \neq 0$ we have a rather different field theory with a first-order time derivative: in this case we can drop the K_2 term as it involves two time derivatives and so is irrelevant with respect to the single time derivative in the K_1 term.

To conclude this discussion, we would like to correlate the above discussion on the distinction between the two universality classes with the behavior of the boson density across the transition. This can be evaluated by taking the derivative of the total free energy with respect to the chemical potential, as is clear from (4):

$$\begin{aligned} \langle \hat{b}_i^\dagger \hat{b}_i \rangle &= -a^d \frac{\partial \mathcal{F}_0}{\partial \mu} - a^d \frac{\partial \mathcal{F}_B}{\partial \mu} \\ &= n_0(\mu/U) - a^d \frac{\partial \mathcal{F}_B}{\partial \mu}, \end{aligned} \tag{38}$$

where $\mathcal{F}_B$ is the free energy resulting from the functional integral over Ψ_B in (34).

In mean-field theory, for $\tilde{r} > 0$, we have $\Psi_B = 0$, and therefore $\mathcal{F}_B = 0$, implying

$$\langle \hat{b}_i^\dagger \hat{b}_i \rangle = n_0(\mu/U), \text{for } \tilde{r} > 0. \tag{39}$$

This clearly places us in a Mott insulator. As argued in Section I A, Eqn. (39) is an exact result.

For $\tilde{r} < 0$, we have $\Psi_B = (-\tilde{r}/u)^{1/2}$, as follows from a simple minimization of $\mathcal{L}_B$; computing the resulting free energy we have

$$\left\langle \hat{b}_i^\dagger \hat{b}_i \right\rangle = n_0(\mu/U) + a^d \frac{\partial}{\partial \mu} \left(\frac{\tilde{r}^2}{2u} \right)$$

$$\approx n_0(\mu/U) + \frac{a^d \tilde{r}}{u} \frac{\partial \tilde{r}}{\partial \mu}. \tag{40}$$

In the second expression, we ignored the derivative of u as it is less singular as $\tilde{r}$ approaches 0; we will comment on the consequences of this shortly. Thus at the transition point at which $K_1 = 0$, by (37) we see that the leading correction to the density of the superfluid phase vanishes, and it remains pinned at the same value as in the Mott insulator. Conversely, for the case $K_1 \neq 0$, the transition is always accompanied by a density change and this is a separate universality class.

We close by commenting on the consequences of the omitted higher order terms in (40) to the discussion above. Consider the trajectory of points in the superfluid with their density equal to some integer n. The implication of the above discussion is that this trajectory will meet the Mott insulator with $n_0(\mu/U) = n$ at its lobe. The relativistic phase transition then describes the transition out of the Mott insulator into the superfluid along a direction tangent to the trajectory of density n. The approximations made above merely amounted to assuming that this trajectory was a straight line.

D. Correlations across the quantum critical point

Let us write action of the field theory in (34) at $K_1 = 0$ in a more general and explicitly relativistic form:

$$\mathcal{S}_\phi = \int d^D x \left\{ \frac{1}{2} \left[(\nabla_x \phi_\alpha)^2 + r \phi_\alpha^2(x) \right] + \frac{u}{4!} \left(\phi_\alpha^2(x) \right)^2 \right\}, \tag{41}$$

where $D = d+1$ is the number of spacetime dimensions, and $\alpha = 1 \ldots N$. The superfluid-insulator transition corresponds to the case $N = 2$, and the superfluid order parameter is $\Psi_B \sim \phi_1 + i\phi_2$. We are interested in the nature of the spectrum as the field theory is tuned from the superfluid to the insulator with r increasing across the quantum critical point at $r = r_c$.

1. *Insulator*

The insulator is present for large and positive r, and here we just use a perturbation theory in u. We compute the correlation function

$$\chi(k) = \int d^D x \, \langle \phi_\alpha(x) \phi_\alpha(0) \rangle \, e^{-ikx}. \tag{42}$$

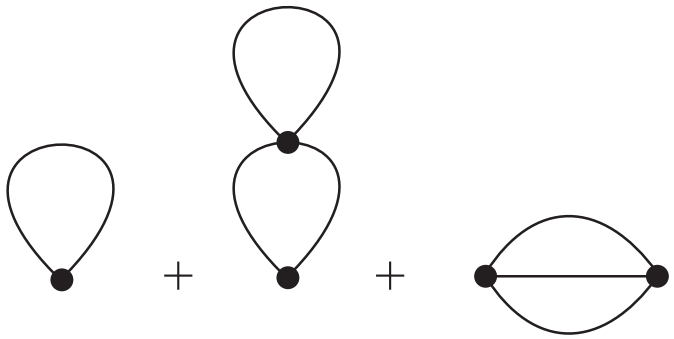

FIG. 2. Diagrams for the self energy to order u^2.

At leading order in u, this is simply $\chi(k) = 1/(k^2+r)$. Analytically continuing this to the quantum theory in d dimensions, we map $k^2 \to c^2k^2 - \omega^2$, and so obtain the retarded response function

$$\chi(k,\omega) = \frac{1}{c^2k^2 + r - (\omega + i\eta)^2} \tag{43}$$

Taking its imaginary part, we have the spectral density

$$\rho(k,\omega) = \frac{\mathcal{A}}{2\varepsilon_k}\left[\delta(\omega - \varepsilon_k) - \delta(\omega + \varepsilon_k)\right] \tag{44}$$

where

$$\varepsilon_k = (c^2k^2 + r)^{1/2} \tag{45}$$

is the dispersion, and we have introduced a 'quasiparticle residue' $\mathcal{A} = 1$. Thus the spectrum consists of $N = 2$ 'particles', and these correspond to the particle and hole excitations of the Mott insulator.

Now let us move beyond the Gaussian theory, and look at perturbative corrections in u. This is represented by the self energy diagrams in Fig. 2. After analytic continuation, we can write the susceptibility in the form

$$\chi(k,\omega) = \frac{1}{c^2k^2 + r - (\omega + i\eta)^2 - \Sigma(k,\omega)} \tag{46}$$

We continue to identify the position of the pole of $\chi(k,\omega)$ (if present) as a function of ω as a determinant of the spectrum of the quasiparticle, and the residue of the pole as the quasiparticle residue $\mathcal{A}$. The real part of the self-energy $\Sigma(k,\omega)$ will serve to modify quasiparticle dispersion relation, and the value of $\mathcal{A}$, but will not remove the pole from real ω axis. To understand possible decay of the quasiparticle, we need to consider the imaginary part of the self energy.

From rather general arguments (in the next paragraph), it is possible to see that

$$\mathrm{Im}\Sigma(k, \omega = \varepsilon_k) = 0 \tag{47}$$

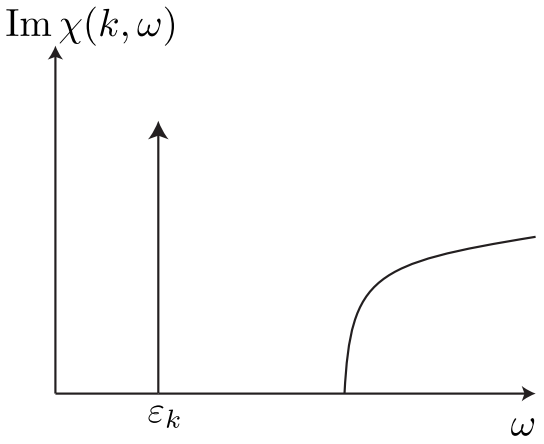

FIG. 3. The spectral density in the paramagnetic phase at $T = 0$ and a small k. Shown are a quasiparticle delta function at $\omega = \varepsilon_k$ and a three-particle continuum at higher frequencies. There are additional n-particle continua ($n \geq 5$ and odd) at higher energies, which are not shown.

at $T = 0$. This can be explicitly verified by a somewhat lengthy evaluation of the diagrams in Fig. 2), and an analytic continuation of the result. An immediate consequence is that the dynamic susceptibility has a delta function contribution which is given exactly by (44). All the higher order corrections only serve to renormalize r, and reduce the quasiparticle residue $\mathcal{A}$ from unity; the dispersion relation continues to retain the form in (45) by relativistic invariance. The stability of the delta function reflects the stability of the single quasiparticle excitations: a quasiparticle with momentum k not too large cannot decay into any other quasiparticle states and still conserve energy and momentum.

However, $\Sigma(k,\omega)$ does have some more interesting consequences at higher ω. We can view ω as the energy inserted by ϕ into the ground state, and so far we have assumed that this energy can only create a quasiparticle with energy ε_k, which has a minimum energy of r. Only for $\omega > pr$, with p integer, can we expect the creation of p particle states. The global O(N) symmetry actually restricts p to be odd, and so the lowest energy multi-particle states that will appear in χ are at $\omega = 3r$. Consonant with this, we find that the self-energy acquires a non-zero imaginary part at zero momentum only for $\omega > 3r$ *i.e.* there is a threshold for 3-particle creation at $\omega = 3r$. The form of $\mathrm{Im}\Sigma(0,\omega)$ at the threshold runs out to

$$\mathrm{Im}\Sigma(0,\omega) \propto \mathrm{sgn}(\omega)\theta(|\omega| - 3r)(|\omega| - 3r)^{(d-1)} \tag{48}$$

for ω around $3r$. Taking the imaginary part of (46), we obtain the generic form of the spectral density shown in Fig. 3.

We now present a simple physical argument for the nature of the threshold singularity in Eq. (48). Just above threshold, we have a particle with energy $3r+\delta\omega$ which decays into 3 particles with energies just above r. The particles in the final state will also have a small momentum, and

so we can make a non-relativistic approximation for their dispersion: $r + c^2k^2/(2r)$. Because the rest mass contributions, r, add up to the energy of the initial state, we can neglect from now. The decay rate, by Fermi's Golden rule is proportional to the density of final states, which yields

$$\begin{aligned}\mathrm{Im}\Sigma(0, 3r + \delta\omega) \propto \int_0^{\delta\omega} d\Omega_1 d\Omega_2 \int \frac{d^dp}{(2\pi)^d}\frac{d^dq}{(2\pi)^d}\delta\left(\Omega_1 - \frac{c^2p^2}{2\sqrt{r}}\right) \\ \times\delta\left(\Omega_2 - \frac{c^2q^2}{2\sqrt{r}}\right)\delta\left(\delta\omega - \Omega_1 - \Omega_2 - \frac{c^2(p+q)^2}{2\sqrt{r}}\right) \\ \sim (\delta\omega)^{(d-1)},\end{aligned} \tag{49}$$

in agreement with (48). We expect this perturbative estimate of the threshold singularity to be exact in all $d \geq 2$.

2. *Quantum critical point*

Evaluation of the susceptibility of the classical field theory (41) at its critical point $r = r_c$ requires a sophisticated resummation of perturbation theory in u using the renormalization group (RG). To order u^2, at the renormalized critical point, perturbation theory in dimension $D = 4$ shows that

$$\chi(k) = \frac{1}{k^2}\left(1 - C_1u^2\ln\left(\frac{\Lambda}{k}\right) + \ldots\right) \tag{50}$$

where Λ is a high momentum cutoff, and C_1 is a positive numerical constant. The RG shows that for $D < 4$ we should exponentiate this series to

$$\chi(k) \sim \frac{1}{k^{2-\eta}} \tag{51}$$

where $\eta > 0$ is the so-called universal anomalous dimension. Precise computations of the value of η are now available for many critical points, included the $N = 2$ case of the field theory (41).

For the quantum critical point, we analytically continue the classical critical point result in (51) to obtain the dynamic susceptibility at the quantum critical point at $T = 0$:

$$\chi(k, \omega) \sim \frac{1}{(c^2k^2 - \omega^2)^{1-\eta/2}} \tag{52}$$

The key feature contrasting this result from (43) is that this susceptibility does *not* have poles on the real frequency axis. Rather, there are branch cuts going out from $\omega = \pm ck$ to infinity. Taking the imaginary part, we obtain a continuous spectral weight at $|\omega| > ck$

$$\mathrm{Im}\chi(k, \omega) \sim \frac{\mathrm{sgn}(\omega)\theta(|\omega| - ck)}{(\omega^2 - c^2k^2)^{1-\eta/2}}; \tag{53}$$

see Fig 4. The absence of a pole indicates that there are no well-defined quasiparticle excitations.

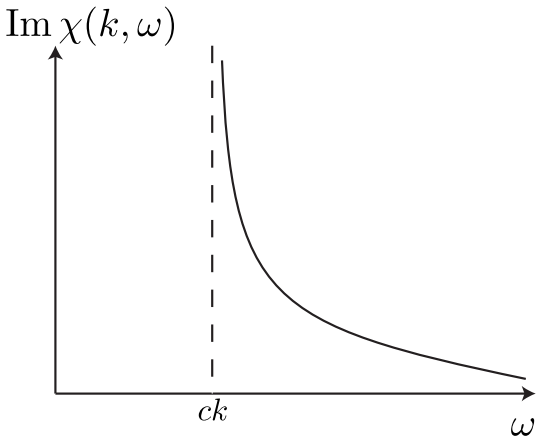

FIG. 4. The spectral density at the quantum critical point. Note the absence of a quasiparticle pole, like that in Fig. 3

Instead we have dissipative continuum of critical excitations at all $|\omega| > ck$: any perturbation will not create a particle-like pulse, but decay into a broad continuum. This is a generic property of a strongly-coupled quantum critical point.

More generally, we can use scaling to describe the evolution of the spectrum as r approaches the critical point at $r = r_c$ from the insulating phase at $T = 0$. Because of the relativistic invariance, the energy gap $\Delta \sim \xi^{-z}$ with $z = 1$, where the correlation length ξ diverges as in the classical model $\xi \sim (r - r_c)^{-\nu}$ (these are definitions of the critical exponents z and ν). In terms of Δ, scaling arguments imply that the susceptibility obey

$$\chi(k,\omega) = \frac{1}{\Delta^{2-\eta}} \widetilde{F}\left(\frac{ck}{\Delta}, \frac{\omega}{\Delta}\right) \tag{54}$$

for some scaling function $\widetilde{F}$. In the insulating phase, the N quasiparticles have dispersion $\varepsilon_k = (c^2k^2 + \Delta^2)^{1/2}$ (the momentum dependence follows from relativistic invariance). Comparing (54) with (44), we see that the two expressions are compatible if the quasiparticle residue scales as

$$\mathcal{A} \sim \Delta^{\eta}; \tag{55}$$

so the quasiparticle residue vanishes as we approach the quantum critical point. Above the quasiparticle pole, the susceptibility of the paramagnetic phase also has p particle continua having thresholds at $\omega = (c^2k^2 + p^2\Delta^2)^{1/2}$, with $p \geq 3$ and p odd. As $\Delta \to 0$ upon approaching the quantum critical point, these multi-particle continua merge to a common threshold at $\omega = ck$ to yield the quantum critical spectrum in (53).

3. *Superfluid state*

Now $r < r_c$, and we have to expand about the ordered saddle point with $\phi_\alpha = N_0 \delta_{\alpha,1}$ where

$$N_0 = \sqrt{\frac{-6r}{u}}. \tag{56}$$

So we write

$$\phi_\alpha(x) = N_0 \delta_{\alpha,1} + \tilde{\phi}_\alpha(x) \tag{57}$$

and expand the action in powers of $\tilde{\phi}_\alpha$.

The first important consequence of the superfluid order is that the dynamic structure factor

$$S(k,\omega) = N_0^2 (2\pi)^{d+1} \delta(\omega) \delta^d(k) + \ldots \tag{58}$$

where the ellipsis represent contributions at non-zero ω. This delta function is easily detectable in elastic neutron scattering, and is a clear signature of the presence of superfluid long-range order.

We now discuss the finite ω contributions to (58). We assume the ordered moment is oriented along the $\alpha = 1$ direction. From Gaussian fluctuations about the saddle point of (41) we obtain susceptibilities which are diagonal in the spin index, with the longitudinal susceptibility

$$\chi_{11}(k,\omega) = \frac{1}{c^2 k^2 - (\omega + i\eta)^2 + 2|r|}, \tag{59}$$

and the transverse susceptibility

$$\chi_{\alpha\alpha}(k,\omega) = \frac{1}{c^2 k^2 - (\omega + i\eta)^2} \quad , \quad \alpha > 1. \tag{60}$$

The poles in these expressions correspond to the $N-1$ spin waves and the "Higgs" particle.

II. ELECTRON HUBBARD MODEL ON THE HONEYCOMB LATTICE

The electron Hubbard model is defined by the Hamiltonian

$$H = -\sum_{i,j} t_{ij} c^\dagger_{i\alpha} c_{j\alpha} + \sum_i \left[-\mu \left(n_{i\uparrow} + n_{i\downarrow} \right) + U_i \left(n_{i\uparrow} - \frac{1}{2} \right) \left(n_{i\downarrow} - \frac{1}{2} \right) \right]. \tag{61}$$

Here $c_{i\alpha}$, $\alpha = \uparrow, \downarrow$ are annihilation operators on the site i of a regular lattice, and t_{ij} is a Hermitian, short-range matrix containing the 'hopping matrix elements' which move the electrons between different lattice sites. The density of electrons is controlled by the chemical potential μ which couples to the total electron density, with

$$n_{i\uparrow} \equiv c^\dagger_{i\uparrow} c_{i\uparrow} \quad , \quad n_{i\downarrow} \equiv c^\dagger_{i\downarrow} c_{i\downarrow}. \tag{62}$$

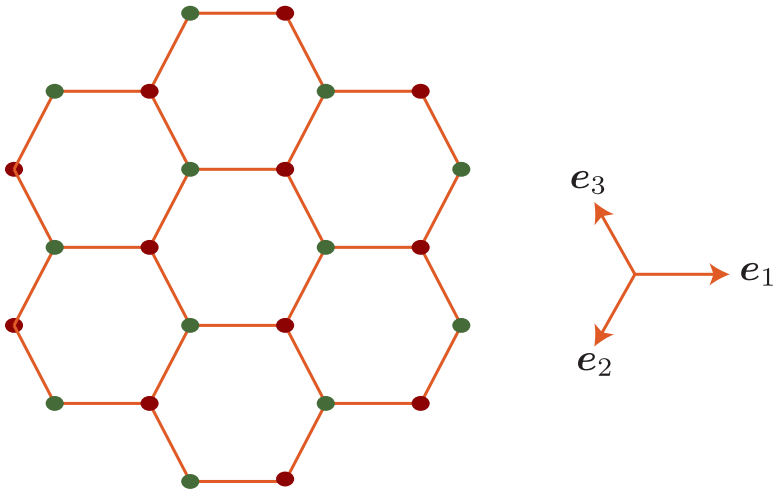

FIG. 5. The honeycomb lattice with its A (green) and B (red) sublattices

The electrons repel each other with an on-site interaction U_i; in most cases we will take $U_i = U$ site-independent, but it will also be useful later to allow for a site-dependent U_i. For completeness, we also note the algebra of the fermion operators:

$$\begin{aligned} c_{i\alpha}c^\dagger_{j\beta} + c^\dagger_{j\beta}c_{i\alpha} &= \delta_{ij}\delta_{\alpha\beta} \\ c_{i\alpha}c_{j\beta} + c_{j\beta}c_{i\alpha} &= 0. \end{aligned} \tag{63}$$

The equations (61), (62), and (63) constitute a self-contained and complete mathematical statement of the problem of the landscape of the Hubbard model. It is remarkable that a problem that is so simple to state has such a rich phase structure as a function of the lattice choice, the fermion density, and the spatial forms of t_{ij} and U_i.

A. Preliminaries

We will consider the Hubbard model (61) with the sites i on locations $\boldsymbol{r}_i$ on the honeycomb lattice shown in Fig. 5 at a density of one electron per site ("half-filling"), so that $\langle n_{i\uparrow}\rangle = \langle n_{i\downarrow}\rangle = 1/2$. Here, we set up some notation allowing us to analyze the geometry of this lattice.

We work with a lattice with unit nearest neighbor spacing. We define unit length vectors which connect nearest-neighbor sites

$$\boldsymbol{e}_1 = (1, 0) \quad , \quad \boldsymbol{e}_2 = (-1/2, \sqrt{3}/2) \quad , \quad \boldsymbol{e}_3 = (-1/2, -\sqrt{3}/2). \tag{64}$$

Note that $\boldsymbol{e}_i \cdot \boldsymbol{e}_j = -1/2$ for $i \neq j$, and $\boldsymbol{e}_1 + \boldsymbol{e}_2 + \boldsymbol{e}_3 = 0$. The lattice can be divided into the A and B sublattices, as shown in Fig. 5. We take the origin of co-ordinates of the lattice at the center of an *empty hexagon*. The A sublattice sites closest to the origin are at $\boldsymbol{e}_1$, $\boldsymbol{e}_2$, and $\boldsymbol{e}_3$, while the B sublattice sites closest to the origin are at $-\boldsymbol{e}_1$, $-\boldsymbol{e}_2$, and $-\boldsymbol{e}_3$.

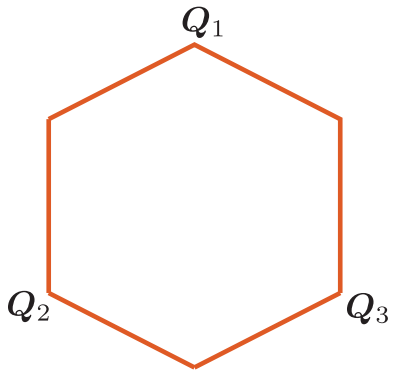

FIG. 6. The first Brillouin zone of the honeycomb lattice.

The unit cell of the hexagonal lattice contains 2 sites, one each from the A and B sublattices. These unit cells form a triangular Bravais lattice consisting of the centers of the hexagons. The triangular lattice points closest to the origin are $\pm(\boldsymbol{e}_1 - \boldsymbol{e}_2)$, $\pm(\boldsymbol{e}_2 - \boldsymbol{e}_3)$, and $\pm(\boldsymbol{e}_3 - \boldsymbol{e}_1)$. The reciprocal lattice is a set of wavevectors $\boldsymbol{G}$ such that $\boldsymbol{G} \cdot \boldsymbol{r} = 2\pi \times$ integer, where $\boldsymbol{r}$ is the center of any hexagon of the honeycomb lattice. The reciprocal lattice is also a triangular lattice, and it consists of the points $\sum_i n_i \boldsymbol{G}_i$, where n_i are integers and

$$\boldsymbol{G}_1 = \frac{4\pi}{3}\boldsymbol{e}_1 \quad , \quad \boldsymbol{G}_2 = \frac{4\pi}{3}\boldsymbol{e}_2 \quad , \quad \boldsymbol{G}_3 = \frac{4\pi}{3}\boldsymbol{e}_3. \tag{65}$$

The unit cell of the reciprocal lattice is called the first Brillouin zone. This is a hexagon whose vertices are given by

$$\boldsymbol{Q}_1 = \frac{1}{3}(\boldsymbol{G}_2 - \boldsymbol{G}_3) \quad , \quad \boldsymbol{Q}_2 = \frac{1}{3}(\boldsymbol{G}_3 - \boldsymbol{G}_1) \quad , \quad \boldsymbol{Q}_3 = \frac{1}{3}(\boldsymbol{G}_1 - \boldsymbol{G}_2), \tag{66}$$

and $-\boldsymbol{Q}_1$, $-\boldsymbol{Q}_2$, and $-\boldsymbol{Q}_3$; see Fig. 6. Integrals and sums over momentum space will implicitly extend only over the first Brillouin zone. This is the 'ultraviolet cutoff' imposed by the underlying lattice structure.

We define the Fourier transform of the electrons on the A sublattice by

$$c_{A\alpha}(\boldsymbol{k}) = \frac{1}{\sqrt{\mathcal{N}}} \sum_{i \in A} c_{i\alpha} e^{-i\boldsymbol{k}\cdot\boldsymbol{r}_i}, \tag{67}$$

where $\mathcal{N}$ is the number of sites on one sublattice; similarly for $c_{B\alpha}$. Note that $c_{A\alpha}(\boldsymbol{k}+\boldsymbol{G}) = c_{A\alpha}(\boldsymbol{k})$: consequently, sums over momentum have to be restricted to the first Brillouin zone to avoid double counting. Thus the inverse of Eq. (67) sums over $\boldsymbol{k}$ in the first Brillouin zone.

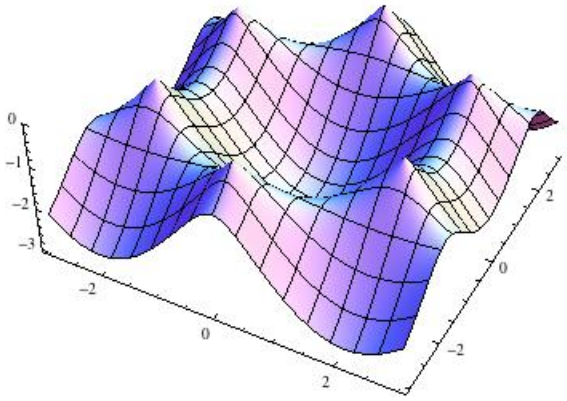

FIG. 7. The lower band of the dispersion in Eq. (70) for $\mu = 0$

B. Semi-metal

We begin with free electrons in the honeycomb lattice, $U = 0$, with only nearest-neighbor electron hopping $t_{ij} = t$. Using Eq. (67), we can write the hopping Hamiltonian as

$$H_0 = -t \sum_{\boldsymbol{k}} \left(e^{i\boldsymbol{k}\cdot\boldsymbol{e}_1} + e^{i\boldsymbol{k}\cdot\boldsymbol{e}_2} + e^{i\boldsymbol{k}\cdot\boldsymbol{e}_3} \right) c^\dagger_{A\alpha}(\boldsymbol{k}) c_{B\alpha}(\boldsymbol{k}) + \text{H.c.} \\ -\mu \sum_{\boldsymbol{k}} \left(c^\dagger_{A\alpha}(\boldsymbol{k}) c_{A\alpha}(\boldsymbol{k}) + c^\dagger_{B\alpha}(\boldsymbol{k}) c_{B\alpha}(\boldsymbol{k}) \right) \tag{68}$$

We introduce Pauli matrices τ^a $(a = x, y, z)$ which act on the A, B sublattice space; then this Hamiltonian can be written as

$$H_0 = \sum_{\boldsymbol{k}} c^\dagger(\boldsymbol{k}) \Big[-\mu - t\Big(\cos(\boldsymbol{k}\cdot\boldsymbol{e}_1) + \cos(\boldsymbol{k}\cdot\boldsymbol{e}_2) + \cos(\boldsymbol{k}\cdot\boldsymbol{e}_3) \Big) \tau^x \\ + t\Big(\sin(\boldsymbol{k}\cdot\boldsymbol{e}_1) + \sin(\boldsymbol{k}\cdot\boldsymbol{e}_2) + \sin(\boldsymbol{k}\cdot\boldsymbol{e}_3) \Big) \tau^y \Big] c(\boldsymbol{k}), \tag{69}$$

where the sublattice and spin indices on the electrons are now implicit: the $c(\boldsymbol{k})$ are 4-component fermion operators.

The energy eigenvalues are easily determined to be

$$-\mu \pm \left| e^{i\boldsymbol{k}\cdot\boldsymbol{e}_1} + e^{i\boldsymbol{k}\cdot\boldsymbol{e}_2} + e^{i\boldsymbol{k}\cdot\boldsymbol{e}_3} \right| \tag{70}$$

and these are plotted in Fig. 7. At half-filling, exactly half the states should be occupied in the ground state, and for the spectrum in Eq. (70) this is achieved at $\mu = 0$.

A crucial feature of any metallic state is the Fermi surface: this is boundary between the occupied and empty states in momentum space. In two spatial dimensions, this boundary is generically a line in momentum space, and this is the case for the dispersion in Eq. (70) for $\mu \neq 0$.

However, for the $\mu = 0$, the honeycomb lattice has the special property that the occupied and empty states meet only at a discrete set of single points in momentum space: this should be clear from the dispersion plotted in Fig. 7. Only 2 of these points are distinct, in that they are not separated by a reciprocal lattice vector $\boldsymbol{G}$. So the half-filled honeycomb lattice has 2 'Fermi points', and realizes a 'semi-metal' phase. The low energy excitations of the semi-metal consist of particles and holes across the Fermi point, and these have a lower density of states than in a metallic phase with a Fermi line. We also note that the Fermi-point structure is protected by a sublattice exchange symmetry: it is not special to the nearest-neighbor hopping model, and it also survives the inclusion of electron-electron interactions.

We obtain a very useful, and universal, theory for the low energy excitations of the semi-metal by expanding (69) in the vicinity of the Fermi points. The distinct Fermi points are present at $\boldsymbol{Q}_1$ and $-\boldsymbol{Q}_1$; all other Fermi points are separated from these two points by a reciprocal lattice vector $\boldsymbol{G}$. So we define continuum Fermi field which reside in 'valleys' in the vicinity of these points by

$$\begin{aligned} C_{A1\alpha}(\boldsymbol{k}) &= \sqrt{A}\, c_{A\alpha}(\boldsymbol{Q}_1 + \boldsymbol{k}) \\ C_{A2\alpha}(\boldsymbol{k}) &= \sqrt{A}\, c_{A\alpha}(-\boldsymbol{Q}_1 + \boldsymbol{k}) \\ C_{B1\alpha}(\boldsymbol{k}) &= \sqrt{A}\, c_{B\alpha}(\boldsymbol{Q}_1 + \boldsymbol{k}) \\ C_{B2\alpha}(\boldsymbol{k}) &= \sqrt{A}\, c_{B\alpha}(-\boldsymbol{Q}_1 + \boldsymbol{k}), \end{aligned} \tag{71}$$

where A is the total area of the honeycomb lattice, and the momentum $\boldsymbol{k}$ is small. The field C is a 8-component continuum canonical Fermi field: the components correspond to spin ($\uparrow$, $\downarrow$), sublattice (A, B), and valley $(1, 2)$ indices. We will also use Pauli matrices which act on the spin (σ^a), sublattice (τ^a), and valley (ρ^a) space.

Inserting Eq. (71) into Eq. (69), we obtain the continuum Hamiltonian

$$H_0 = \int \frac{d^2k}{4\pi^2} C^\dagger(\boldsymbol{k}) \Big(v\tau^y k_x + v\tau^x \rho^z k_y \Big) C(\boldsymbol{k}), \tag{72}$$

where $v = 3t/2$. From now on we rescale time to set $v = 1$. Diagonalizing Eq. (72), we obtain the relativistic spectrum

$$\pm \sqrt{k_x^2 + k_y^2}, \tag{73}$$

which corresponds to the values of Eq. (70) near the Fermi points.

The relativistic structure of H_0 can be made explicit by rewriting it as the Lagrangian of massless Dirac fermions. Define $\overline{C} = C^\dagger \rho^z \tau^z$. Then we can write the Euclidean time (τ) Lagrangian density of the semi-metal phase as

$$\mathcal{L}_0 = \overline{C} \left(\partial_\tau \gamma_0 + \partial_x \gamma_1 + \partial_y \gamma_2 \right) C \tag{74}$$

where ω is the frequency associated with imaginary time, and the Dirac γ matrices are

$$\gamma_0 = -\rho^z \tau^z \quad \gamma_1 = \rho^z \tau^x \quad \gamma_2 = -\tau^y. \tag{75}$$

In addition to relativistic invariance, this form makes it clear the free-fermion Lagrangian has a large group of 'flavor' symmetries that acts on the 8×8 fermion space and commute with the γ matrices. Most of these symmetries are not obeyed by higher-order gradients, or by fermion interaction terms which descend from the Hubbard model.

Let us now turn on a small repulsion, U, between the fermions in the semi-metal. Because of the point-like nature of the Fermi surface, it is easier to determine the consequences of this interaction here than in a metallic phase with a Fermi line of gapless excitations. We can use traditional renormalization group (RG) methods to conclude that a weak U is irrelevant in the infrared. Consequently, the semi-metal state is a stable phase which is present over a finite range of parameters.

C. Antiferromagnet

Although a small U is irrelevant, new phases can and do appear at large U. To see this, let us return to the lattice Hubbard model in Eq. (61), and consider the limit of large $U_i = U$. We will assume $\mu = 0$ and half-filling in the remainder of this section.

At $U = \infty$, the eigenstates are simple products over the states on each site. Each site has 4 states:

$$|0\rangle \quad , \quad c^\dagger_{i\uparrow}|0\rangle \quad , \quad c^\dagger_{i\downarrow}|0\rangle \quad , \quad c^\dagger_{i\uparrow}c^\dagger_{i\downarrow}|0\rangle, \tag{76}$$

where $|0\rangle$ is the empty state. The energies of these states are $U/4$, $-U/4$, $-U/4$, and $U/4$ respectively. Thus the ground state on each site is doubly-degenerate, corresponding to the spin-up and spin-down states of a single electron. The lattice model has a degeneracy of $2^{2\mathcal{N}}$, and so a non-zero entropy density (recall that $\mathcal{N}$ is the number of sites on one sublattice).

Any small perturbation away from the $U = \infty$ limit is likely to lift this exponential large degeneracy. So we need to account for the electron hopping t. At first order, electron hopping moves an electron from one singly-occupied site to another, yielding a final state with one empty and one doubly occupied site. This final state has an energy U higher than the initial state, and so is not part of the low energy manifold. So by the rules of degenerate perturbation theory, there is no correction to the energy of all the $2^{2\mathcal{N}}$ ground states at first order in t.

At second order in t, we have to use the effective Hamiltonian method. This performs a canonical transformation to eliminate the couplings from the ground states to all the states excited by energy U, while obtaining a modified Hamiltonian which acts on the $2^{2\mathcal{N}}$ ground states. This method is described in text books on quantum mechanics. The resulting effective Hamiltonian is the Heisenberg antiferromagnet:

$$H_J = \sum_{i<j} J_{ij} S^a_i S^a_j \quad , \quad J_{ij} = \frac{4t^2_{ij}}{U}, \tag{77}$$

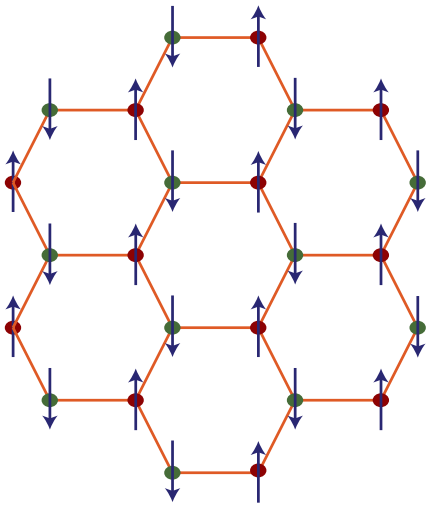

FIG. 8. The large U state with antiferromagnetic (Néel) order.

where J_{ij} is the exchange interaction and S_i^a are the spin operators on site i

$$S_i^a = \frac{1}{2} c_{i\alpha}^\dagger \sigma_{\alpha\beta}^a c_{i\beta}. \tag{78}$$

Note that these spin operators preserve the electron occupation number on every site, and so act within the subspace of the $2^{2\mathcal{N}}$ low energy states. The Hamiltonian H_J lifts the macroscopic degeneracy, and the entropy density of the new ground state will be zero.

Although we cannot compute the exact ground state of H_J on the honeycomb lattice with nearest-neighbor exchange, numerical studies [3] leave little doubt to its basic structure. The ground state is adiabatically connected to that obtained by treating the S_i^a as classical vectors in spin space: it has antiferromagnetic (or Néel) order which breaks the global SU(2) spin rotation symmetry, by a spontaneous polarization of the spins on opposite orientations on the two sublattices

$$\eta_i \langle S_i^a \rangle = N^a, \tag{79}$$

where $\eta_i = 1$ ($\eta_i = -1$) on sublattice A (B), and N^a is the vector Néel order parameter; see Fig. 8. Classically this state minimizes the exchange coupling in Eq. (77) because $J_{ij} > 0$. Quantum fluctuations for spin $S = 1/2$ reduce the spontaneous moment from its classical value, but a non-zero moment remains on the honeycomb lattice.

What is the electronic excitation spectrum in the antiferromagnet? To determine this, it is useful to write the Néel order parameter in terms of the continuum Dirac fields introduced in Section II B. We observe

$$\sum_i \eta_i S_i^a = \sum_{\boldsymbol{k}} \left(c_{A\alpha}^\dagger \sigma_{\alpha\beta}^a c_{A\beta} - c_{B\alpha}^\dagger \sigma_{\alpha\beta}^a c_{B\beta} \right) = \int \frac{d^2k}{4\pi^2} C^\dagger \tau^z \sigma^a C \tag{80}$$

Thus the Néel order parameter N^a is given by the fermion bilinear

$$N^a = \left\langle C^\dagger \tau^z \sigma^a C \right\rangle = \left\langle \overline{C} \rho^z \sigma^a C \right\rangle, \tag{81}$$

and the vacuum expectation value (VEV) is non-zero in the antiferromagnet. We can expect that electron-electron interactions will induce a coupling between the fermion excitations and this VEV in the low energy Hamiltonian for the Néel phase. Choosing Néel ordering in the z direction

$$N^a = N_0 \delta_{az}, \tag{82}$$

we anticipate that H_0 in Eq. (72) is modified in the Néel phase to

$$H_N = \int \frac{d^2k}{4\pi^2} C^\dagger(\boldsymbol{k}) \Big(\tau^y k_x + \tau^x \rho^z k_y - \lambda N_0 \tau^z \sigma^z \Big) C(\boldsymbol{k}), \tag{83}$$

where λ is a coupling determined by the electron interactions, and we have assumed Néel order polarized in the z direction. This effective Hamiltonian will be explicitly derived in the next subsection. We can now easily diagonalize H_N to deduce that the electronic excitations have energy

$$\pm \sqrt{k_x^2 + k_y^2 + \lambda^2 N_0^2}. \tag{84}$$

This is the spectrum of massive Dirac fermions. So the Fermi point has disappeared, and an energy gap has opened in the fermion excitation spectrum. In condensed matter language, the phase with antiferromagnetic order is an insulator, and not a semi-metal: transmission of electronic charge will require creation of gapped particle and hole excitations.

D. Quantum phase transition

We have now described a semi-metal phase for small U, and an antiferromagnetic insulator for large U. Both are robust phases, whose existence has been reliably established. We now consider connecting these two phases at intermediate values of U [3].

We can derive the field theory for this direct transition either by symmetry considerations, or by an explicit derivation from the Hubbard model. Let us initially follow the second route. We start with the Hubbard Hamiltonian in Eq. (61), use the operator identity (valid on each site i):

$$U \left(n_\uparrow - \frac{1}{2} \right) \left(n_\downarrow - \frac{1}{2} \right) = -\frac{2U}{3} S^{a2} + \frac{U}{4}. \tag{85}$$

Then, in the fermion coherent state path integral for the Hubbard model, we apply a 'Hubbard-Stratonovich' transformation to the interaction term; this amounts to using the identity

$$\begin{aligned} &\exp\left(\frac{2U}{3} \sum_i \int d\tau S_i^{a2} \right) \\ &= \int \mathcal{D} X_i^a(\tau) \exp\left(- \sum_i \int d\tau \left[\frac{3}{8} X_i^{a2} - \sqrt{U} X_i^a S_i^a \right] \right) \end{aligned} \tag{86}$$

The fermion path integral is now a bilinear in the fermions, and we can, at least formally, integrate out the fermions in the form of a functional determinant. We imagine doing this temporarily, and then look for the saddle point of the resulting effective action for the X_i^a. At the saddle-point we find that the lowest energy is achieved when the vector has opposite orientations on the A and B sublattices. Anticipating this, we look for a continuum limit in terms of a field φ^a where

$$X_i^a = \eta_i \varphi^a \tag{87}$$

Using Eq. (80), the continuum limit of the coupling between the field φ^a and the fermions in Eq. (86) is given by

$$X_i^a c_{i\alpha}^\dagger \sigma_{\alpha\beta}^a c_{i\beta} = \varphi^a C^\dagger \tau^z \sigma^a C = \varphi^a \overline{C} \rho^z \sigma^a C \tag{88}$$

From this it is clear that φ^a is a dynamical quantum field which represents the fluctuations of the local Néel order, and

$$\langle \varphi^a \rangle \propto N^a. \tag{89}$$

Now we can take the continuum limit of all the terms in the coherent state path integral for the lattice Hubbard model and obtain the following continuum Lagrangian density

$$\mathcal{L} = \overline{C} \gamma_\mu \partial_\mu C + \frac{1}{2}\left[(\partial_\mu \varphi^a)^2 + s \varphi^{a2} \right] + \frac{u}{24} \left(\varphi^{a2} \right)^2 - \lambda \varphi^a \overline{C} \rho^z \sigma^a C \tag{90}$$

This is a relativistic quantum field theory for the 8-component fermion field C and the 3-component real scalar φ^a, related to the Gross-Neveu-Yukawa model; the scalar part is the same as the $N = 3$ case of the superfluid-insulator field theory in (41). We have included gradient terms and quartic in the Lagrangian for φ^a: these are not present in the derivation outlined above from the lattice Hubbard model, but are clearly induced by higher energy fermions are integrated out. The Lagrangian includes various phenomenological couplings constants (s, u, λ); as these constants are varied, $\mathcal{L}$ can describe *both* the semi-metal and insulating antiferromagnet phases, and also the quantum critical point between them.

Note that the matrix $\rho^z \sigma^a$ commutes with all the γ_μ; hence $\rho^z \sigma^a$ is a matrix in "flavor" space. So if we consider C as 2-component Dirac fermions, then these Dirac fermions carry an additional 4-component flavor index.

The semi-metal phase is the one where φ^a has vanishing vacuum expectation value (VEV). In mean-field theory, this appears for $s > 0$. The φ^a excitations are then massive, and these constitute a triplet of gapped 'spin-excitons' associated with fluctuations of the local antiferromagnetic order. The Dirac fermions are massless, and represent the Fermi point excitations of the semi-metal.

The Néel phase has a non-zero VEV, $\langle \varphi^a \rangle \neq 0$, and appears in mean-field theory for $s < 0$. Here the Dirac fermions acquire a gap, indicating that the Fermi point has vanished, and we are now in an insulating phase. The fluctuations of φ are a doublet of Goldstone modes ('spin waves') and a longitudinal massive Higgs boson.

Finally, we are ready to address the quantum critical point between these phases. In mean-field theory, this transition occurs at $s = 0$. As is customary in condensed matter physics, it is useful to carry out an RG analysis near this point. Such an analysis can be controlled in an expansion in $1/N$ (where N is the number of fermion flavors) or $(3-d)$ (where d is the spatial dimensionality). The main conclusion of such analyses is that there is an RG fixed point at which the φ^{a2} is the only relevant perturbation. Non-linearities such as λ and u all reach stable fixed point values of order unity. This non-trivial fixed point implies that the physics of the quantum critical point is highly non-trivial and strongly coupled. The RG fixed point is scale- and relativistic-invariant, and this implies that it is also conformally invariant. Thus the quantum critical point is described by a CFT in 2+1 spacetime dimensions: a CFT3.

We will not describe the critical theory in any detail here. However, we will note some important characteristics of correlation functions at the quantum critical point. The electron Green's function has the following structure

$$\left\langle C(k,\omega); C^\dagger(k,\omega)\right\rangle \sim \frac{i\omega + k_x\tau^y + k_y\tau^x\rho^z}{(\omega^2 + k_x^2 + k_y^2)^{1-\eta_f/2}} \tag{91}$$

where $\eta_f > 0$ is the *anomalous dimension* of the fermion. This leads to a fermion spectral density which has no quasiparticle pole: thus the quantum critical point has no well-defined quasiparticle excitations. This distinguishes it from both the semi-metal and insulating antiferromagnetic phases that flank it on either side: both had excitations with infinitely-sharp quasiparticle peaks. Similar anomalous dimensions appear in the correlations of the bosonic order parameter φ^a.

---

[1] M. P. A. Fisher, P. B. Weichman, G. Grinstein, and D. S. Fisher, "Boson localization and the superfluid-insulator transition," Phys. Rev. B **40**, 546 (1989).

[2] J. Negele and H. Orland, *Quantum many-particle systems*, Frontiers in physics (Addison-Wesley Pub. Co., 1988).

[3] F. F. Assaad and I. F. Herbut, "Pinning the Order: The Nature of Quantum Criticality in the Hubbard Model on Honeycomb Lattice," Physical Review X **3**, 031010 (2013), arXiv:1304.6340 [cond-mat.str-el].